

April, 1995

Spontaneous symmetry breaking and the formation of columnar structures in the primary visual cortex II

— Local organization of orientation modules —

Kengo Yamagishi

Lab for Neural Modeling

email: k-yama@hep-th.phys.s.u-tokyo.ac.jp

ABSTRACT

Self-organization of orientation-wheels observed in the visual cortex is discussed from the view point of topology. We argue in a generalized model of Kohonen's feature mappings that the existence of the orientation-wheels is a consequence of Riemann-Hurwitz formula from topology. In the same line, we estimate partition function of the model, and show that regardless of the total number N of the orientation-modules per hypercolumn the modules are self-organized, without fine-tuning of parameters, into definite number of orientation-wheels per hypercolumn if N is large.

Keywords— Orientation columns, Visual cortex, Self-organizing feature maps, Neural networks, Orientation singularities, Riemann-Hurwitz theorem, Spontaneous symmetry breaking, Topological maps

1 Introduction

Among various columns observed in cortical surface, orientation columns in primary visual area V1 exhibit one of the most attractive structural organization. Here expanding our previous study (Yamagishi, 1994, referred to as I hereafter), we would like to investigate the mechanism of the self-organization of these orientation columns from the view point of spontaneous symmetry breaking. In so doing we hope that we will get deeper understanding of the role of these columns not only in the context of self-organization but also in the information processing problem in visual cortex.

Since the first discovery by Hubel and Wiesel (1977 for a survey), these distributed localized area of iso-orientation preference have attracted people's attention. In their earlier model (see Figure 1), based on their experimental data, although they are not conclusive, the columns are considered (proposed) as some form of slabs embedded between ocular dominance boundary walls. Each slab is assigned detectors with specific orientation preference. However, in the recent experiments, as more precise data have become available, more detailed structure of this organization is becoming to emerge.

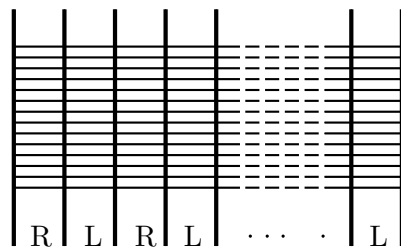


Figure 1. Ice-cube model of orientation columns by Hubel and Wiesel. Orientation columns are regularly embedded in R, L ocular dominance area.

In one of the most recent data Blasdel (1992; see also Obermayer *et al.*, 1993) showed in higher precision that the orientation columns are basically organized according to two classes of structural basis: point singularities and fractures. The general feature near the ocular dominance boundary wall still remain the same as in the previous results; the orientation and ocular dominance walls intersect in right angles. It has also been shown that these structural bases — singular points and/or fractures — typically stay between the ocular dominance walls with the average number ($3 \sim 4$) per hypercolumn. This structure constitutes a unit module (approximately $1\text{mm} \times 1\text{mm}$ square region on the cortical surface in the case of monkeys) that

contains a right set of feature-detector cells of color-, orientation-, spatial frequency-information, etc. for an associated segment of visual field (corresponding to $0.8^\circ \times 0.8^\circ$ near fovea region).

The purpose of our study is first to consider the precise meaning of modular organization where the feature space consists of continuous (or infinite) degrees of freedom like in this case. In principle, we would need infinite number of column-modules if we enforce modular organization à la Hubel and Wiesel in full precision. At the same time we do not know the minimum resolution of orientation angles, or even whether such concept at the orientation-column level is meaningful or not. In the next section after reviewing some morphology of this columnar organization, we propose a “statistical definition of orientation modules” to address this. There the module boundaries are not defined as definite objects as in classical picture of Hubel and Wiesel, rather they are defined only statistically.

Quantitative analysis of this scheme is made in §§3-4. We use generalized Kohonen’s feature mapping algorithm (Kohonen, 1982, 1989) to check this idea. Models of the same class have been used before for the ocular dominance columns (Obermayer *et al.*, 1992, 1990; Yamagishi 1994). In our model (I) we added an extra one-dimensional (feature) space to the ordinary Kohonen that is frequently used in two-dimensional self-organization problem on cortical surface, and analyzed its continuum limit with respect to spacing between neurons. Introducing a certain regularization method to handle rather singular “winner-takes-all” mechanism, we derived that the lowest stable state is a solitonic kink-anti-kink state corresponding to the ocular dominance domain-walls. Here we follow basically the same strategy. Added feature space, however, is not a line interval $[-1, 1]$ but a compact space S^1 including its interior that represents the orientation degrees of freedom with each probability indicated by the radial distance from the center of the S^1 . [The center of this feature space represents “no orientation preference”.] In order to derive a global configuration of the orientation columns, we would need a full fledged system that includes both ocular and orientation degrees of freedom. In this paper, however, we would like to address more fundamental questions: why the orientation singularities appear, and how these are related to the (statistical definition of) orientation modules proposed in this paper. For the latter purpose only, we do not need feature space terms related to the ocular dominance columns.

We restrict our model in one hypercolumn area only. [We would like to address global organization problem in future publications.] The solitonic states in

this case correspond basically to harmonic maps with respect to retinotopic coordinates. In two-dimensions (and in a simple topology) they are just linear combinations of holomorphic and anti-holomorphic mappings. As an analytic continuation from global topographic mapping of retina to visual cortex, which is roughly approximated by a holomorphic (and anti-holomorphic) mapping, we choose holomorphic mappings to describe orientation columns in one ocular domain of the hypercolumn (and anti-holomorphic ones for the other ocular domain). In modular organization these mappings are basically one-to-many. (The image in each orientation column is a replication of the original one mapped from retina onto hypercolumn region in the layer 4C.) Quite generally in a holomorphic mapping from one compact space to another compact space, this global information (multiplicity or “mapping degree”) gives rise to some restriction on the local structure of the mapping, i.e., existence and number of singularities. We will show that the orientation singularities correspond to these singularities. We would like to explain this point in detail in §3.

In §4, we derive statistical distribution function (partition function) of the above mappings in the path integral formalism. (See e.g. our previous work I.) The result is written in a summation with respect to the mapping degree and the number of singularities. We will see that this precisely corresponds to our statistical definition of the orientation modules. This is because the size (accordingly the iso-orientation width) of the module changes according to the selection of the mapping degrees from the layer 4C to the layers 2+3; the mapping degree is large if the iso-orientation width is narrow, and is small in the converse case. The partition function contains all these contributions in the statistical sum.

One interesting result in our calculation is that this partition function takes maximum value at finite number of singularities regardless of the mapping degree if the latter is large enough. This implies that in average there exist stable, definite number of orientation wheels in the hypercolumn anywhere on the cortical surface, regardless of the size of the orientation modules. That agrees with what actually observed on the cortical surface.

Finally we discuss some future issues in §5.

2 Definition of orientation modules

In this section we present our precise definition of orientation modules, starting with their fundamental anatomical descriptions on which our theory is based.

Our main focus in this paper is the orientation columns in layers 2+3 observed in macaque visual cortex[†]. Major inputs to neurons in these orientation columns come from layer 4[‡]. Typical dendrites of the orientation detector neurons extend $200 \sim 500\mu\text{m}$, that is about the scale of the ocular dominance width, in all directions almost uniformly. Lateral spread of the interlaminar axons from layer 4C is $300\mu\text{m} \sim 400\mu\text{m}$ right before the dendritic input into cells in layers 2+3. Thus precise topographic mapping from retina established in the layer 4C is maintained there only in the scale larger than hypercolumn size (Fitzpatrick *et al.*, 1985). Some like-orientation columns in neighboring hypercolumns are interconnected like clusters via rather long (a few mm up to several mm) collateral axonal arbors from each orientation cell across the ocular walls (Gilbert and Wiesel, 1983, 1989). Some cross-orientation (inhibitory) interactions between such clusters are also observed (Matsubara *et al.*, 1987; McGuire *et al.*, 1991).

The receptive field profile of each constituent (simple) orientation detector cell ranges typically around $0.5^\circ \times 0.5^\circ \sim 1.5^\circ \times 1.5^\circ$ at central visual field. That has been compared to 2D Gabor filters, and with an appropriate adjustment of parameters a good agreement is demonstrated (Jones and Palmer, 1987).*

In recent high precision experimental data (Blasdel, 1992), observed iso-orientation domains are organized based on two structural centers: point singularities and fractures. Distribution of the iso-orientation domains around the singular point is either increasing or decreasing with respect to the orientation preference angles. In average, those clock-wise or anti-clock wise orientation centers distribute evenly in every hypercolumn.

Statistically among clock wise (or anti-clock wise) orientation centers the position of an orientation preference within the orientation wheels seems to be at random, namely, in average one orientation preference (say, 3:00 direction in visual field) occurs at any angle in the orientation wheels on the cortical surface, although the orientation-preference changes monotonically increasing or decreasing within one wheel (with a certain increment depending on the experimental set-up). It should also be empha-

[†]Localized areas of orientation preference are also observed in other layers (5, 6) and visual area (e.g. V2 (area 18) Bonhoeffer *et al.*, 1993). However, we would like to restrict our theory only to layers 2+3 for the sake of precaution.

[‡]Some from 4A, 4B, and some directly from 4C α , 4C β and LGN.

*These results are not conclusive. Other possibilities are also known (e.g. Hawken and Parker, 1987).

sized that the iso-orientation domain is not separated into more than two pieces within one wheel — it occurs only once. This plays important role later.

This monotonic change of orientation preference is interrupted and cut (or stopped) by “fractures” where a portion of iso-orientation domains from other wheels intersects.

The shape of the iso-orientation domains in each wheel does not seem to be definitive. It tends to be elongated in the direction of the radial direction from the singularity on the cortical surface, but is not definitive. It involves some artifact, i.e., how one defines iso-orientation width. There is almost no correlation between those shapes and preferred orientation directions of the cells as well as positions of the iso-orientation domains in the wheel.

From these observations we can safely conclude the followings. Firstly, the filtering mechanism of each orientation information, via e.g. 2D-Gabor filter-like structures, seems to be independent of the self-organization mechanism (since the shape of the iso-orientation domain is rather arbitrary and its position within orientation wheels does not depend on the orientation preference of the visual field).

Secondly, it looks quite unlikely that total monotonic change of iso-orientation preferences ranging over 180° in one orientation wheel plays any essential role in the orientation detection (since the fractures can interrupt it arbitrarily).

Therefore, this self-organization is something that only assembles together the cells of similar functionality semi-locally but with no definite global order. The existence of the singularities itself looks mere consequence of this organization mechanism rather than some immediate necessity for information processing strategy of orientations. In contrast, the monotonic change (either just increasing or decreasing, but not like increasing and then decreasing) of the orientation preference in the semi-local region seems to play important role.

Now, based upon these observations, in the remainder of this section we would like to present our definition of the “modular organization” in the case at hand, where feature space consists of some continuous degrees of freedom. In the original idea of Hubel and Wiesel, each orientation slab, the “module” of the orientation detection, was assumed to receive replicated (but somewhat distorted) image projected over the hypercolumn size region where it resides, and each of the slabs was assigned detectors with a specific orientation preference. Then those orientation slabs associated to various possible orientation directions were supposed to fill up the entire hypercolumn region as in Figure 1. In this way, 3-dimensional information (i.e., a totality of

“orientations at every image points”) was considered to be processed. However, the “orientation” has full continuous (infinite) degrees of freedom. If we enforce this scheme in full precision, we need infinite number of orientation columns and nerve cells.

However, we also know the following fact. If one tries to detect an orientation precisely, one has to sacrifice positional precision that is parallel to that orientation direction (Daugmann, 1985). This holds not only in each detector cell level but in general. Hence in the limit of the finest precision of the orientation the projected image of the hypercolumn eventually reduces to one-dimensional degrees of freedom perpendicular to the orientation direction. Namely, in the detectable information space, the information is not fully 3-dimensional one. We need a certain trade-off between the orientation and the positional precision parallel to it.

Taking into account this, we consider here the information-processing scheme and its associated modular organization as in the following. “The module of iso-orientation (and its boundary) in the classical sense of Hubel and Wiesel[‡] is not definite”. Namely, we propose that the extent of the module virtually changes according to the image one is concentrating on. If one tends to focus on (via higher cortical function) information about the sharpness of an orientation direction of an edge rather than whose position (e.g. case of a long edge), then only the outputs from those detector cells that fall into quite narrow range of orientation are selected as if those cells constitute one “orientation module” associated with that orientation. In that case the “orientation module” encompasses a very thin domain of iso-orientation region. On the contrary in the case one tends to extract informations about orientation with moderate precision at a special, precise point (e.g. very short edge — say, less than a quarter degree $\approx 1\text{mm}@25\text{cm}$ -distance sight) in a visual field, then the informations from moderately narrow range of orientation preferences are selected as if those orientation cells constitute one orientation module. Namely, the orientation module is dynamically configured, and there is no definite boundary between orientation modules.

State it differently, here the size of the orientation module is statistically defined. There is no definite (or classical) modular organization in the sense of Hubel and Wiesel.

[‡]Here the “global order” of the iso-orientation slabs as seen in Figure 1 is not the point of our attention.

To achieve this multiple projection scheme, almost all the orientation detector cells have to receive inputs from all axonal arbors projected from the layer 4 within the same hypercolumn that they belong to. The results from observation on axon morphology, as we briefly sketched before about layers 4C and its superficial laminae, are not inconsistent with this hypothesis.

The unexpected support for this scheme actually comes from the real organization of the orientation columns. The necessary organizational structure to attain this scheme is firstly the semi-local continuity of the orientation preference in a size no larger than, say, 30 degrees of orientation width. We do not need global or 180° continuity. But most important, among other things, is a forgetful, simple fact that the iso-orientation patch should not be separated into more than two pieces in one orientation wheel, namely, the preference angle should not change in such a fashion that it increases and then decreases continuously. At least from one fracture to the next fracture the preference angle has to change monotonically within one orientation wheel, either increasing or just decreasing, otherwise our scheme does not work.

This scheme itself does not exclude global order of orientation domains, e.g., the organization shown in Figure 1. But we do not need such high global order — semi-local order is enough to attain this scheme, and that is more plausible if the cells are self-organized on a non-genetic basis.

3 Role of holomorphicity

In this section, we would like to present our model to describe local-organizations and formulations of our orientation modules. We use a model basically of the same class as in our previous work I, i.e., a generalization of Kohonen’s self-organizing feature maps. To establish notations, let us briefly recall its formulations.

3.1 The model

Let $\vec{w}(\vec{r}, \tau)$ be a 2-component vector-valued function defined on every cortical point \vec{r} at time step τ . We assume that each $\vec{w}(\vec{r}, \tau)$ represent a point in retina’s field E . Then the set of vectors $\{\vec{w}(\vec{r}, \tau) | \vec{r} \in F \equiv \text{a set of cortical points}\}$ defines neural connections between the retinal surface and the visual cortex, and gives rise to a mapping of retinal image onto the visual cortex. Here, in addition, we consider a complex-valued function $w_{\mathcal{O}}(\vec{r}, \tau)$ (where $|w_{\mathcal{O}}(\vec{r}, \tau)| \leq 1$) that belongs to a hypothetical orientation feature-

space D^2 , a flat disc of radius 1 with its boundary circle S^1 . We can think of $w_{\mathcal{O}}(\vec{r}, \tau) \in D^2$ as indicating a preference of the orientation detector cell placed at a cortical point \vec{r} , whose preferred orientation angle is directed to $\arg[w_{\mathcal{O}}(\vec{r}, \tau)]$ with probability $|w_{\mathcal{O}}(\vec{r}, \tau)|$. (Namely, the cell has a polarization $|w_{\mathcal{O}}(\vec{r}, \tau)|$ in the preferred orientation $\arg[w_{\mathcal{O}}(\vec{r}, \tau)]$. We assume no orientation preference if $|w_{\mathcal{O}}(\vec{r}, \tau)| = 0$.) Then the pair $(\vec{w}(\vec{r}, \tau), w_{\mathcal{O}}(\vec{r}, \tau))$ represents a retinal information mapped to the cortical point \vec{r} together with the orientation-preference at that point.

We update this system using the following learning rule. We start with a random configuration of $\mathbf{w} = (\vec{w}(\vec{r}, \tau), w_{\mathcal{O}}(\vec{r}, \tau))$ at the time step $\tau = 0$, and repeat the two-step process stated below upon every presentation of the data $\boldsymbol{\xi} = (\vec{\xi}, \xi_{\mathcal{O}}) \in E \otimes S^1$. ($\xi_{\mathcal{O}}$ is a complex number of modulus 1 specified later.) The first step is a so-called ‘‘winner-takes-all’’:

[UPDT:1] Select the winning point \vec{r}^* on the cortical surface where the retinal vector $\mathbf{w}^* \equiv (\vec{w}(\vec{r}^*, \tau), w_{\mathcal{O}}(\vec{r}^*, \tau))$ is closest to the data $\boldsymbol{\xi} = (\vec{\xi}, \xi_{\mathcal{O}})$ presented at the time τ .

Here the (distance)² between two points $\mathbf{w}_a, \mathbf{w}_b$ in the feature-data space is defined as

$$d(\mathbf{w}_a, \mathbf{w}_b) \equiv \|\vec{w}_a - \vec{w}_b\|^2 + \sigma_0^2 h(w_{\mathcal{O}_a}, w_{\mathcal{O}_b}). \quad (1)$$

The second term that indicates a perturbative effect from the ordinary Kohonen becomes significant only in the scale smaller than σ_0 . We take σ_0 the typical size of orientation columns, which is far smaller than retinotopic organization (\sim scale of the visual area V1). We also assume expansion:

$$h(w_{\mathcal{O}_a}, w_{\mathcal{O}_b}) = g_1 |w_{\mathcal{O}_a} - w_{\mathcal{O}_b}|^2 + g_2 |w_{\mathcal{O}_a} - w_{\mathcal{O}_b}|^4 + \dots, \quad (2)$$

where $g_1 (\sim \mathcal{O}(1)) \gg |g_2| \gg \dots$ are numerical constants taking real values. As we see later, this choice of $h(w_{\mathcal{O}_a}, w_{\mathcal{O}_b})$ respects a chiral symmetry of orientation wheels at global scale, namely, the clock-wise and anti-clock-wise wheels appear evenly in global average.

The second step is the updating rule for the vector configuration $\mathbf{w} \equiv (w_i(\vec{r}, \tau)) = (\vec{w}(\vec{r}, \tau), w_{\mathcal{O}}(\vec{r}, \tau))$ following

[UPDT:2]

$$\langle \Delta w_i(\vec{r}, \tau) P(\boldsymbol{\xi}, \tau) \rangle_{\boldsymbol{\xi}} = -\epsilon(\tau) \delta \mathcal{E}[\mathbf{w}] / \delta w_i(\vec{r}, \tau),$$

$$\Delta w_i(\vec{r}, \tau) \equiv w_i(\vec{r}, \tau + 1) - w_i(\vec{r}, \tau).$$

Here $\langle \cdots P(\boldsymbol{\xi}, \tau) \rangle_{\boldsymbol{\xi}} \equiv \sum_{\boldsymbol{\xi}} \cdots P(\boldsymbol{\xi}, \tau)$ stands for an average over the given probability function $P(\boldsymbol{\xi}, \tau)$ of the presented data $\boldsymbol{\xi}$, $\epsilon(\tau)$ (> 0) is the certain (decreasing) learning coefficient $\epsilon(\tau) \downarrow 0$ as $\tau \rightarrow \infty$, and $\mathcal{E}[\mathbf{w}]$ is an energy function that we specify in the following. This process stops if the system reaches to a stationary point $\delta\mathcal{E}[\mathbf{w}]/\delta w_i(\vec{r}, \tau) = 0$.

The energy function we employ is a perturbed one from what frequently used in the retinotopic self-organization problem. Let $\Lambda_{\vec{r}, \vec{r}^*} = \lambda^{-1} \exp(-\|\vec{r} - \vec{r}^*\|^2/2\sigma_0^2)$ be a lateral correlation that signifies a short excitatory signal from the winning point \vec{r}^* with λ being a positive numerical constant, and let a data-profile $\mathcal{F}_{\vec{r}^*}[\mathbf{w}]$ at that point be defined as in

$$\mathcal{F}_{\vec{r}^*}[\mathbf{w}] = \left\{ \boldsymbol{\xi} \equiv (\vec{\xi}, \xi_{\mathcal{O}}) \in E \otimes S^1 \mid \forall \vec{r} \in F, d(\boldsymbol{\xi}, \mathbf{w}(\vec{r}^*, \tau)) \leq d(\boldsymbol{\xi}, \mathbf{w}(\vec{r}, \tau)) \right\}. \quad (3)$$

The latter corresponds to a set of data which a cortical cell at the point \vec{r}^* can handle under the given configuration of \mathbf{w} . Using these quantities, the energy function $\mathcal{E}[\mathbf{w}]$ is written as:

$$\mathcal{E}[\vec{w}] = \frac{1}{2} \sum_{\vec{r}, \vec{r}^*} \Lambda_{\vec{r}, \vec{r}^*} \sum_{\boldsymbol{\xi} \in \mathcal{F}_{\vec{r}^*}[\mathbf{w}]} P(\boldsymbol{\xi}, \tau) \left(\|\vec{\xi} - \vec{w}(\vec{r}, \tau)\|^2 + \sigma_0^2 h(\xi_{\mathcal{O}}, w_{\mathcal{O}}(\vec{r}, \tau)) \right). \quad (4)$$

As we noted in our previous work I, retaining only g_1 -term ($g_2 = g_3 = \cdots = 0$) in $h(\xi_{\mathcal{O}}, w_{\mathcal{O}}(\vec{r}, \tau))$ reduces this system to the standard Kohonen for the mapping of feature space $E \otimes D^2$ onto the cortical surface F .

We consider the time-development of this system under presentation of a data set $\{\vec{\xi}, \xi_{\mathcal{O}}\}$ with the probability $P(\vec{\xi}, \xi_{\mathcal{O}}; \tau) = P(\vec{\xi})$, namely, we use totally random, homogeneous inputs with respect to the orientation preference. We also restrict our orientation data $\xi_{\mathcal{O}} = e^{i\pi k/N}$ ($k = 0, 1, \dots, N - 1$) for some positive integer N . This means in particular that each of our input data is always 100% polarized to one of finite possible orientation directions.

The local symmetry concerned here is unitary group $U(1)$

$$w_{\mathcal{O}}(\vec{r}) \rightarrow e^{i\gamma(\vec{r})} w_{\mathcal{O}}(\vec{r}), \quad \xi_{\mathcal{O}} \rightarrow e^{i\gamma(\vec{r})} \xi_{\mathcal{O}} \quad (5)$$

instead of \mathbb{Z}_2 appeared in our previous work I. In this equation $\gamma(\vec{r})$ is an arbitrary real function of \vec{r} . Our energy function (4) is easily seen to be form-invariant under the transformation (5).

3.2 The picture for the ground state

First we would like to recall results from retinotopy problem derived without our perturbative term $\sigma_0^2 h(\xi_{\mathcal{O}}, w_{\mathcal{O}}(\vec{r}, \tau))$. For this purpose it is convenient to go over to continuum limit of the model in the final convergent phase. We can assume the lateral correlation width σ_0 very small. Then the equation for a stationary state $\delta\mathcal{E}[\mathbf{w}]/\delta w_i = 0$ can be approximated as follows.

At the final convergent stage, the set $\mathcal{F}_{\vec{r}^*}[\mathbf{w}]$ is almost uniquely given by one point set $\mathcal{F}_{\vec{r}^*}[\mathbf{w}] = \{\vec{\xi} = \vec{w}(\vec{r}^*, \tau)\}$. Hence we have

$$0 = \frac{\delta\mathcal{E}[\mathbf{w}]}{\delta w_i(\vec{r})} = \int \Lambda_{\vec{r}, \vec{r}^*} (w_i(\vec{r}) - w_i(\vec{r}^*)) P(\vec{w}(\vec{r}^*)) d^2\vec{w}(\vec{r}^*).$$

Writing $\vec{r}^* = \vec{r} + \vec{\epsilon}$, and taking into account the Gaussian factor $\Lambda_{\vec{r}, \vec{r}^*}$ of small width σ_0 , we obtain in the limit $\sigma_0 \rightarrow 0$

$$0 = \partial^2 w_i(\vec{r}) + 2 \{P(\vec{w}(\vec{r})) \cdot J(\vec{w}(\vec{r}))\}^{-1} \partial_\rho \{P(\vec{w}(\vec{r})) \cdot J(\vec{w}(\vec{r}))\} \partial_\rho w_i(\vec{r}). \quad (6)$$

Here $J(\vec{w}(\vec{r}))$ is a Jacobian

$$J(\vec{w}(\vec{r})) = \varepsilon^{\alpha\beta} \partial_\alpha w^1(\vec{r}) \partial_\beta w^2(\vec{r})$$

with anti-symmetric symbol $\varepsilon^{12} = -\varepsilon^{21} = 1$, arising from the change of integration variables $d^2\vec{w}(\vec{r}^*) \rightarrow d^2\vec{\epsilon}$. The stationary state has to satisfy the equation (6).

It is pointed out (Ritter and Schulten, 1986) that for the retinotopic organization an appropriate solution is given in terms of the harmonic form satisfying

$$\partial^2 w_i(\vec{r}) = 0. \quad (7)$$

In fact given a probability distribution on the retinal data

$$P(\vec{\xi}(\vec{r})) \propto J^{-1}(\vec{w}(\vec{r})) \Big|_{\vec{w}(\vec{r})=\vec{\xi}}, \quad (8)$$

one can get a logarithmic mapping relation that solves the equations (6), (7),

$$r^1 + ir^2 = \log(w^1(\vec{r}) \pm iw^2(\vec{r}) + \alpha), \quad (9)$$

between the visual cortex and the retinal surfaces. This mapping, from half disk region of \vec{w} to upper half plane of \vec{r} , gives a crude approximation to the observed results. In equation (9) the choice of the sign \pm depends on which ocular (left or right eye) information one considering, and α is the constant of length scale of fovea

region. We presume that the probability distribution (8) is provided via function $\vec{w}(\vec{r})$ satisfying (9) at the start of the iteration of the learning steps.

Next we consider the case with the perturbative term $\sigma_0 h(\xi_{\mathcal{O}}, w_{\mathcal{O}}(\vec{r}, \tau))$ included, and restrict our attention to one hypercolumn area only — that is about 5 to 10 times larger than the scale of the orientation columns σ_0 . Then we can still apply the similar approximation method as we used in deriving the result (6) to the energy function (4). In general this time the winning point \vec{r}^* is not one-to-one with $\vec{w}(\vec{r}^*)$ even in the final convergent phase. Instead, the “winner-takes-all” [UPDT:1] ensures one-to-one correspondence relation between \vec{r}^* and $(\vec{w}(\vec{r}^*), w_{\mathcal{O}}(\vec{r}^*))$. Generally, since our orientation data take only discrete values $\xi_{\mathcal{O}} = e^{i\pi k/N}$ ($k = 0, 1, \dots, N - 1$), $w_{\mathcal{O}}(\vec{r}^*)$ approaches locally constant functions at the final convergent stage, i.e., $|\xi_{\mathcal{O}} - w_{\mathcal{O}}(\vec{r}^*)| \rightarrow 0$ (where local continuity of $w_{\mathcal{O}}(\vec{r})$ is assumed). Thus the data-feature space points $(\vec{w}(\vec{r}^*), w_{\mathcal{O}}(\vec{r}^*))$, in which the first coordinates $\vec{w}(\vec{r}^*)$ is the same, are distinguished by the discrete “labeling” $w_{\mathcal{O}}(\vec{r}^*)$. Then our data profile $\mathcal{F}_{\vec{r}^*}$ consists of a set of pair $\{(\vec{w}(\vec{r}^*), w_{\mathcal{O}}(\vec{r}^*))\}$ at the convergent phase. Using this fact, we can expand our energy function (4) at lowest order of σ_0 as follows:

$$\Delta \mathcal{E} \propto \lambda^{-1} \sigma_0^2 \int_{\text{hypercolumn}} P(\langle \vec{w} \rangle) |J(\vec{v}(\vec{r}))| \left((\partial \vec{v}(\vec{r}))^2 + g_1 (\partial w_{\mathcal{O}}(\vec{r}))^2 \right) d^2 \vec{r}. \quad (10)$$

This gives an extra energy per hypercolumn. Recall that λ is a measure for strength of the lateral correlation $\Lambda_{\vec{r}, \vec{r}^*}$. To avoid confusion we write $\sigma_0 \vec{v}(\vec{r}) \equiv \vec{w}(\vec{r}) - \langle \vec{w} \rangle$ instead of $\vec{w}(\vec{r})$ that was used for global retinotopic problem. The global retinotopic solution $\langle \vec{w} \rangle$ (equation (9)) and the probability $P(\langle \vec{w} \rangle)$ are treated almost constant within the hypercolumn region. In the above expression (10) we have to be careful about sign change of the Jacobian $J(\vec{v})$. This is because in comparison to the previous case the relation between \vec{r}^* and $\vec{v}(\vec{r}^*)$ is not one-to-one; the Jacobian could vanish and even change sign, giving rise to folding maps (see the followings).

In order to get a picture for the ground state let us consider the possible situations that lower the energy (10). First of all, all terms in the energy function are non-negative. The lowest value in the integrand is attained when the Jacobian factor $J(\vec{v}(\vec{r}))$ vanishes and the locally constant function $w_{\mathcal{O}}(\vec{r})$ does not change its value $|\partial w_{\mathcal{O}}| \neq \infty$ there. In 2-dimensional mappings the vanishing Jacobian $J(\vec{v}(\vec{r})) = 0$ occurs in the following cases.

(i) The case $\text{rank}[J] = 1$

(i-a) $J(\vec{v})$ changes sign in the neighborhood of $J(\vec{v}) = 0$.

(i-b) $J(\vec{v})$ does not change sign in the neighborhood of $J(\vec{v}) = 0$.

(ii) The case $\text{rank}[J] = 0$

Here, abusing notations, we write the Jacobian $J(\vec{v}) = \det(\partial v_i(\vec{r})/\partial r_j) \equiv \det[J]$. The case (i) corresponds to line singularities. The equation of the singular line is determined by solving $J(\vec{v}) = 0$. In detail, the subcase (i-a) indicates that there is a fold along that line since changing the sign of the Jacobian implies alteration of orientation of the surface. The subcase (i-b) means existence of a sort of degeneracy

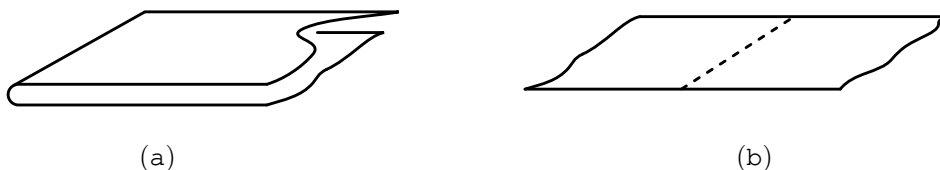


Figure 2. Examples of a folding map (a) and a line degeneracy (b). Slightly separated appearance of the leaves in the folding map (a) is for the sake of visibility. These mappings can occur when the Jacobian $J(\vec{v}) = \det(\partial v_i(\vec{r})/\partial r_j)$ of the mapping $\vec{v}(\vec{r})$ between retinal and the corresponding cortical surfaces vanishes.

of the mapping $\vec{v}(\vec{r})$ along the line, but no folds. The simple example is shown in the Figure 2. The sample mapping $(v_1(\vec{r}), v_2(\vec{r})) = (r_1^2, r_2)$ in Figure 2(a) exhibits a fold along the line $v_1 = r_1 = 0$. Figure 2(b) shows a degenerate line singularities along $v_1 = r_1 = 0$ in the mapping $(v_1(\vec{r}), v_2(\vec{r})) = (r_1^3, r_2)$.

In our model (10) the type (i-a) singularity or a fold does not occur unless the orientation function $w_{\mathcal{O}}(\vec{r})$ changes its (locally constant) value when one crosses that folding line. This is because the “winner-takes-all” [UPDT:1] prohibits multiple winning points $(\vec{w}(\vec{r}_i^*), w_{\mathcal{O}}(\vec{r}_i^*)) = (\vec{w}(\vec{r}_j^*), w_{\mathcal{O}}(\vec{r}_j^*))$, $(\vec{r}_i^* \neq \vec{r}_j^*)$ that could otherwise occur

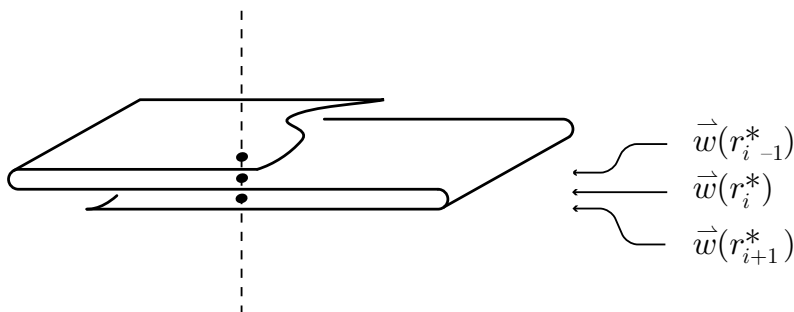


Figure 3. Multiple winning points on a folding cover. When one encounters a folding cover of the retinal surface, because of the “winner-takes-all” rule each leaf $i - 1, i, i + 1$ of the folding cover has to have different orientation preference $w_{\mathcal{O}}(\vec{r}^*)$.

on leaves i, j of the folded region. (See Figure 3.) To prevent this at least each leaf has to be organized to have different labels $w_{\mathcal{O}}(\vec{r}_i^*) \neq w_{\mathcal{O}}(\vec{r}_j^*)$ for $i \neq j$. Then the contribution to our energy function (10) along these folding lines is ($J = 0$) times ($|\partial w_{\mathcal{O}}|^2 = \infty$). We encountered similar situation in the previous work I. We can employ a similar regularization method in this case to make this product finite. The lower energy configuration is such that the total length of the folding lines is allowable shortest. However, this argument is based solely on the neighborhood of the folding lines. Actually the folding maps are unlikely to occur. This is because, following the analysis in the previous work I, locally at quite small scale the lower energy mapping is almost identity mapping $\vec{w}(\vec{r}) \sim \vec{r}$ up to conformal rescaling. Unless one feeds the system with non-homogeneous data in such a way that a certain localized region gets mapped to be twisted with opposite orientation, the folding is quite exceptional situation. If it happens, the folding line could be observed like “fractures”.

In contrast, the type (i-b) singularity is rather harmless. It can occur basically anywhere. In practice in computer simulations (or in real neuronal circuits) this type of line singularity, which manifests itself as thin accumulations of points onto a line in continuum theory, will not have observable effect, since the system is discretized. Unless the lattice spacing (or resolution) is quite small, the effect will be negligible. If it produces observable accumulation (or a certain area fails to grow and collapses to a line by some reason), then this line would also resemble the “fracture”.

However, it if occurs at the boundary of iso-orientation region ($|\partial w_{\mathcal{O}}| = \infty$), it contributes to the energy function in the same way as in the previous case (i-a). In fact, this case is precisely the situation at the boundary of each ocular domains in Figure 2(a) of I. There we described the regularized value of the product ($J(\vec{w}) = 0$) \cdot ($|\partial w_{\mathcal{O}}| = \infty$) as kink energy. The contribution of this to the energy (10) gets lowered if the total length of the iso-orientation boundary is allowable, shortest.

Here we should also point out that in the ground state the iso-orientation boundary $|\partial w_{\mathcal{O}}| = \infty$ only occurs at those points where the Jacobian vanishes $J(\vec{v}) = 0$. (Otherwise, the energy (10) diverges and the corresponding probability distribution vanishes.) Therefore, the iso-orientation boundary typically does not have unnecessarily wiggly shape, rather it is close to geodesic lines.

Finally, we have the case (ii) $\text{rank}[J]=0$. In this case the condition $J(\vec{v}) = 0$ determines a point, leading us to a point-singularity or an intersection of line-singularities. Before discussing the property of the point-singularity, we briefly consider the property of non-singular region $J(\vec{v}) \neq 0$. There $w_{\mathcal{O}}(\vec{r})$ has to be almost constant

($\partial w_{\mathcal{O}} \approx 0$) in the ground state. Then the remaining first term in energy (10) exhibits the same dynamics as the retinotopy problem analyzed before. Since the probability $P(\langle \vec{w} \rangle)$ is constant here, we can reasonably assume so is $J(\vec{v})$, and $\vec{v}(\vec{r})$ is locally harmonic $\partial^2 \vec{v} = 0$. This could only be violated near the singular lines and points where $J(\vec{v})$ approaches 0.

Generally, using complex coordinates $z = r^1 + ir^2$, $\Phi = v^1 + iv^2$, the harmonic function here can be written in a linear combination of holomorphic and anti-holomorphic functions:

$$\Phi = \Phi_0(z) + \Phi_1(\bar{z}).$$

Since at global scale the mapping is given in terms of an holomorphic (or anti-holomorphic) functions (9), let us assume for the moment that this property persists at hypercolumn scale. Namely, we consider $\Phi(z)$ as some sort of analytic continuation from global retinotopic function (9). This assumption is consistent with the mapping without folds.

In 2-dimensions the holomorphic mapping is (locally) a conformal mapping. With an appropriate coordinate transformation, the point singularities (of the type we are considering) can always be put into a standard form, e.g, near the singular point at z_0 it reads

$$\Phi(\vec{v}(\vec{r})) = (z - z_0)^{b(z_0)}. \quad (11)$$

Here the $b(z_0)$ (≥ 1) is called a ramification index at that point. (If $b(z_0) = 1$, it represents a regular point $J(\vec{v}(z_0)) \neq 0$.) This defines a branched covering of the retinal surface near the point $\vec{v}(z_0)$; on the corresponding cortical surface the $b(z_0)$ sheets of the covering come together in fan-shape. By the same reason in the case of the folding maps (cf. Figure 3), the “winner-takes-all” ensures a different labeling $w_{\mathcal{O}}(z)$ on each covering sheet in the ground state. (Therefore, the ramification index $b(z_0)$ is smaller than possible orientation specifications N , i.e. $b(z_0) \leq N$.) Thus there should exist singular lines ($J(\vec{v}) = 0$) of type (i-b) near this system.

The associated feature-space function $w_{\mathcal{O}}(z)$ is determined by minimizing the energy (10) near that point. Standard variation with respect to $w_{\mathcal{O}}(z)$ gives the equation:

$$\partial_z \bar{\partial}_z w_{\mathcal{O}}(z) + J(\vec{v})^{-1} \partial_z J(\vec{v}) \cdot \bar{\partial}_z w_{\mathcal{O}}(z) + J(\vec{v})^{-1} \bar{\partial}_z J(\vec{v}) \cdot \partial_z w_{\mathcal{O}}(z) = 0.$$

Substituting (11) into $J(\vec{v}) = |\partial_z \Phi(z)|^2 - |\bar{\partial}_z \Phi(z)|^2$, we have

$$\partial_z \bar{\partial}_z w_{\mathcal{O}}(z) + \frac{b-1}{z} \bar{\partial}_z w_{\mathcal{O}}(z) + \frac{b-1}{\bar{z}} \partial_z w_{\mathcal{O}}(z) = 0, \quad (12)$$

where we put $z_0 = 0$, $b(z_0) = b$ for simplicity. Since $w_{\mathcal{O}}(z)$ is the locally constant function, this is always satisfied in almost all the places except near singular points $J(\vec{v}) = 0$. (See Figure 4.) As stated above each covering-sheet has different label $w_{\mathcal{O}} = e^{i\pi k_i/N}$, $k_i \neq k_j$. Since the distance between the two points in the feature space

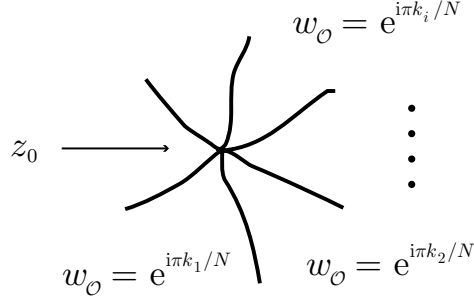


Figure 4. Labeling of a multiple covering (unfolded view). As in the case of folding covers (Figure 3) the “winner-takes-all” rule enforces different labeling $w_{\mathcal{O}} = e^{i\pi k_i/N}$, $k_i \neq k_j$, for each covering-sheet of retinal surface in general multiple coverings.

is $|e^{i\pi k_i/N} - e^{i\pi k_j/N}| = 2 \sin[\pi(k_i - k_j)/2N]$, the neighbouring labels k_i and $k_{i\pm 1}$ is expected to take close values under the [UPDT:2]. In the case $N \rightarrow \infty$ and the ramification index $b \rightarrow \infty$ (recall $N \geq b$) where the each covering sheet looks thin fan-shaped region on the cortical surface, each k_i approaches continuous function with respect to the index i , — or equivalently the the function of $\arg[z]$.

In fact, one can solve equation (12) generally as follows. Since equation (12) can be rewritten as

$$\partial_z \bar{\partial}_z (z^{b-1} \bar{z}^{b-1} w_{\mathcal{O}}(z)) = (b-1)^2 (z\bar{z})^{-1} (z^{b-1} \bar{z}^{b-1} w_{\mathcal{O}}(z))$$

with $\partial_z \bar{\partial}_z$ being simply a 2-dimensional Laplacian, we can write down its general solution as a linear combination of products of azimuthal functions $e^{2i\gamma\phi} = (z/\bar{z})^\gamma$ and radial ones $f_\gamma(\rho)$ (where $\rho^2 = z\bar{z}$) for various spectra γ . Explicitly we have

$$w_{\mathcal{O}}(z) = \int_{-\infty}^{\infty} d\gamma A(\gamma) \left(\frac{z}{\bar{z}}\right)^\gamma \cdot (z\bar{z})^{-(b-1) + \sqrt{\gamma^2 + (b-1)^2}}, \quad (13)$$

where $A(\gamma)$ is an unknown coefficient function (that would be determined by solving global system including ocular terms in the energy function). In this equation we have discarded the other possible term $(z/\bar{z})^\gamma (z\bar{z})^{-(b-1) - \sqrt{\gamma^2 + (b-1)^2}}$, that is divergent as $z \rightarrow 0$, since $|w_{\mathcal{O}}(z)| \leq 1$ by definition. Among the expansion terms in equation (13), only one term is dominant at $z \approx 0$; that is given by

$$w_{\mathcal{O}}(z) \approx A(\gamma_{|\min|}) \left(\frac{z}{\bar{z}}\right)^{\gamma_{|\min|}} \cdot (z\bar{z})^{\gamma_{|\min|}^2/2(b-1)}. \quad (14)$$

Here $\gamma_{|\min|}$ is the minimum positive or maximum negative value of γ (whichever the absolute value is smaller) for which the expansion coefficient function $A(\gamma)$ does not vanish. We also took a leading term in $b \rightarrow \infty$ limit. Depending on the signature of $\gamma_{|\min|}$, $w_{\mathcal{O}}(z)$ gives clock-wise or anti-clock-wise configuration of the orientation detector cells. [If $A(0) \neq 0$, then $\gamma_{|\min|} = 0$, i.e., the feature function $w_{\mathcal{O}}(z)$ is constant. Following preceding argument below equation (12), this is not the case, however.] Therefore, we conclude generally that in association to singular points $\Phi(z) \sim z^b$ we have clock-wise or anti-clock-wise orientation wheels, and that each orientation module organized around the singular point is one of $b(z_0)$ -tuple covering of the local area of the retina. Since in equation (14) $w_{\mathcal{O}}(z)$ is a continuum limit $N \rightarrow \infty$ of $w_{\mathcal{O}} = e^{i\pi k_j/N}$, the $\gamma_{|\min|}$ has to satisfy $-1/4 \leq \gamma_{|\min|} \leq 1/4$.

Now what so remarkable about working in (piecewise) holomorphic environment is that there exist a celebrated topological formula by Riemann and Hurwitz that relates the ramification indices $b(z)$ to the Euler characteristics of the surfaces under consideration. Specifically, let $\chi(E)$ and $\chi(F)$ be the Euler characteristics of the surfaces E and F , and $b(z)$ be the ramification index at $z \in F$ associated to the covering $\Phi(z) : F \rightarrow E$, then it states the relation

$$\chi(F) = n \cdot \chi(E) - \sum_{z \in F} (b(z) - 1). \quad (15)$$

In this equation n is the mapping degree (or the number of the total coverings) of the map $\Phi(z)$, i.e.,

$$n = \sum_{z \in \Phi^{-1}(w_0)} b(z)$$

for an (arbitrary) point w_0 in E . (For an accessible exposition on this formula, see, e.g., Griffiths, P. and Harris, J., Principles of Algebraic Geometry, John Wiley & Sons, pp. 216-218 (1978).) In the case at hand E and F are small square regions of retina and visual cortex, respectively, and we can take $\chi(E) = 1$ and $\chi(F) \approx$ number of blocks of continuously changing orientation area (see next section). Plainly speaking, here the mapping degree is just the total number of orientation modules within one hypercolumn. Since the ramification index equals one at almost all the points on the cortical surface F (i.e., ordinary points), the summation $\sum_{z \in F} (b(z) - 1)$ in equation (15) is actually a finite sum over singular points to which orientation modules come together. The most important thing that equation (15) tells us is the “existence” of singularities, namely, since the Euler characteristics are stated as above, as long as the number of orientation module is larger than that of blocks of continuously

changing orientation area within one hypercolumn ($n > \chi(F)$), there must exist points with non-trivial ramification index $b(z) > 1$. Following the preceding analysis on the associated feature space function $w_{\mathcal{O}}(z)$, that would imply the existence of the orientation wheels.

Unfortunately, global configuration of these singular points are beyond the scope of this formula. However, we can consider statistical distribution function (a partition function) of possible mixed branched- and unbranched-coverings of retinal surfaces, and write them down as a function of number of singular points. We will do this in the next section.

To summarize, we have discussed various possible situations that lower the energy (10). Semi-global structure at the scale of hypercolumn size can be sketched as follows. Although there is a difference in 2-dimensional Gaussian factor $\Lambda_{\vec{r}, \vec{r}^*}$ here and the 1-dimensional one used in the previous calculation in I, basic organization-structure in arbitrary one-dimensional cross-section of the present case will bear resemblance to the kink-anti-kink configuration (Figure 2(a) of I). Namely, dominance by only one feature (i.e., $w_{\mathcal{O}}(z) = \text{constant}$) over a broad range of the cortical surface is unlikely to occur. This includes the case $w_{\mathcal{O}}(z) = 0$ where there is no orientation preference, since these configurations merely raise the total energy by the same reason as in 1-dimensional case, i.e., the non-trivial contribution from the second term in energy (4) gives large value proportional to the area of such regions. Instead the lower energy configuration is such that the various locally constant values $w_{\mathcal{O}}(z) = e^{i\pi k_j/N}$ are distributed over the surface in such a way that their boundaries (where $|\partial w_{\mathcal{O}}| = \infty$) become (allowable) shortest and consistent with the distributed orientation wheels. The reason for this is that the boundaries contribute finite positive energy after the regularization of the product with Jacobian ($J(\vec{v}) = 0$) $\cdot (|\partial w_{\mathcal{O}}|^2 = \infty)$, which is the same situation as in I where the corresponding product was referred to as kink energy.

We also discussed the structure of point singularities in detail, and how orientation wheels (both clock-wise and anti-clock-wise) occur in association with the point singularities of the Jacobian $J(\vec{v}) = 0$. The monotonic (increasing or decreasing) change of the orientation preference angle was also shown to take place as locally energy-minimizing configurations. Most remarkable is the number of singularities that was found to follow the celebrated Riemann-Hurwitz formula.

4 Partition function

In this section we would like to estimate statistical distribution function of our model associated to the lower energy configurations described in the previous section. This corresponds to evaluation of path integral (see, e.g., our previous work I)

$$\begin{aligned} \mathcal{Z} &\sim \int \mathcal{D}\mathbf{v} e^{-\Delta\mathcal{E}[\mathbf{v}]} \\ &\sim \sum_{\mathbf{v}} [\text{multiplicity of the covering map } \mathbf{v}] e^{-\Delta\mathcal{E}[\mathbf{v}]} \end{aligned}$$

for the dominant contributions. As we discussed before the covering map here is specified by its mapping degree $n = N$, the total number of branch points I , their positions z_i , and associated ramification indices $b(z_i)$. Most of this section is devoted to the counting problem of the multiplicities of these mappings for the given data $(N, I, b(z_i))$.

4.1 Unbranched and branched coverings of retinal surface

Although in this paper our main concern is the covering maps of an area of retina, that is topologically equivalent to a disk, we first start with an unbranched covering of a torus for its illustrative purpose. We write a plaquette for a torus, assuming identification (Figure 5(a)) of like-labeled edges in each side. An unbranched N -sheeted covering is a collection of N such objects glued together (Figure 5(b)) along like-labeled edges. There are many varieties to construct this type of covering surfaces (including ones with disconnected components). In order to cover the original torus, one identifies each horizontal edges, and then wraps up the torus with the resulting

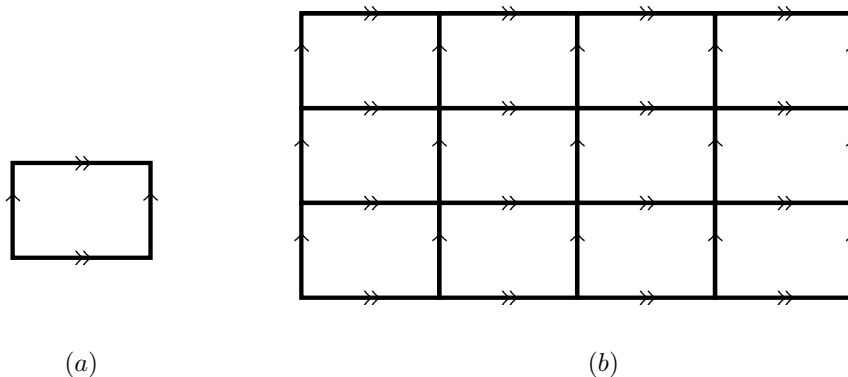
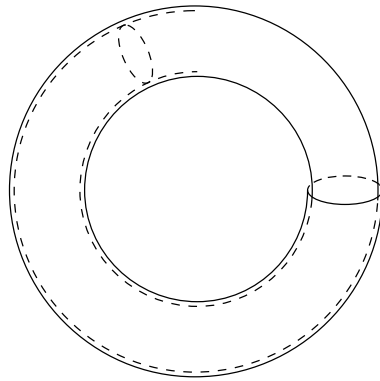


Figure 5. An unbranched covering of a torus. We write a plaquette for a torus, assuming identification of like-labeled edges in each side (Figure (a)). An unbranched N -sheeted covering (Figure (b)) is a collection of N such objects glued together along like-labeled edges. Then one

identifies each horizontal edges, and wraps up the torus with the resulting cylinder by putting one end of the cylinder in the other end until the circumferences match up with the original torus (Figure (c)).



(c)

Figure 5. (cont'd).

cylinder by putting one end of the cylinder in the other end until the circumferences match up with the original torus (Figure 5(c)). In this way, every point of the original torus are covered precisely N times. The Riemann-Hurwitz formula (15) is trivially satisfied.

Next we consider a branched covering of a sphere (S^2). We start with a 2-sheeted unbranched covering of S^2 . Just as in previous case the unbranched covering corresponds to a simple double wrapping of S^2 ; every points are covered twice in this covering. We name the covering sheets “1” and “2”. To make from this a branched covering, we pick two points (A, B) on the sphere and cut the covering sheets along the straight line connecting these two points (Figure 6(a)). Then we identify one edge of the sheet “1” with the edge of the sheet “2” on the other side of the cut and the remaining edge of the sheet “1” with that of the sheet “2”, i.e., identification of the like-labeled edges p, q in Figure 6(a). The resulting covering is branched; the two points A, B we picked are branch points (of index 2).

To see its topologically equivalent surface, we peel off the outer sphere, and paste it back along the edges p, q as prescribed (Figure 6(b)). Then we end up with an object in sphere topology. The Riemann-Hurwitz formula (15) is satisfied since the Euler indices $\chi(E) = \chi(F) = 2$ for the sphere, $n = 2$ (double covering), and the ramification indices $b = 2$ at both branch points (A, B). [In the case of simple unbranched covering the Euler characteristic of the covering surface is just the multiple of the original one by the number of coverings.]

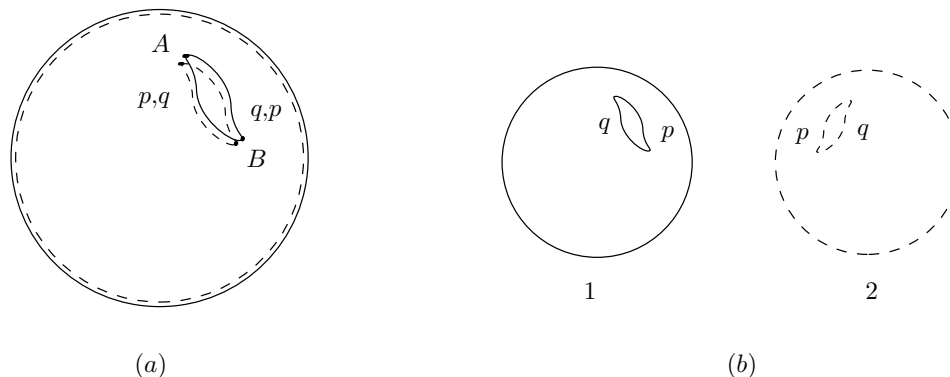


Figure 6. A branched covering of a sphere. We start with a 2-sheeted unbranched covering of S^2 , and name the covering sheets “1” and “2”. To make from this a branched covering, we pick two points (A, B) on the sphere and cut the covering sheets along the straight line connecting these two points (Figure (a)). Then we identify one edge of the sheet “1” with the edge of the sheet “2” on the other side of the cut and the remaining edge of the sheet “1” with that of the sheet “2”, i.e., we identify the like-labeled edges p, q in the Figure (a). The resulting covering is branched; the two points A, B we picked are branch points (of index 2). To see its topologically equivalent surface, we peel off the outer sphere, and paste it back along the edges p, q as prescribed (Figure (b)).

An example of the corresponding analytic expression for this covering is the mapping $z \mapsto w \equiv z^2 (\in \mathbb{C} \cup \{\infty\})$, where the singularities (of the ramification index 2) occur at the north ($z = \infty$) and south ($z = 0$) poles of the (stereo-graphically projected) sphere.

The branch points on this sphere are characterized as follows. We draw a small circle on the sphere surrounding one of the branch point. Obviously, going around once on the circle takes one from the covering-sheet “1” (or “2”) to “2” (or “1”), and a repetition of this process brings one back to the starting position. The same is true with regard to the other branch point. One can think of this process as an action of transpositional element (12) in the symmetric group \mathcal{S}_2 on the labels “1, 2” of the covering-sheets.

For the case 3-sheeted branched covering with two branch points, we can repeat the similar construction, using identification rules as shown in Figure 7(a). The Figure shows the sectional view from the north pole. It is easy to see that the resulting branched cover has again sphere topology. An example of the corresponding analytic mapping is $z \mapsto w \equiv z^3$ with the ramification indices $b(0) = b(\infty) = 3$. In this case, the branch points are characterized by the permutational element (123) of

symmetric group \mathcal{S}_3 . Figure 7(b) shows another gluing rule in which mixed branched and unbranched coverings occur. This time the branch points are characterized by the transposition (12)(3) of the \mathcal{S}_3 . In Figure 7(c) in another construction we separated out the two branch points with ramification indices 3 in Figure 7(a) into four branch points with ramification indices 2. [The total branching number is invariant in this process: $(3 - 1) \times 2 = (2 - 1) \times 4$.] The new branch points are characterized by (12)(3) and (1)(23) of the symmetric group \mathcal{S}_3 , respectively, associated to each gluing edge.

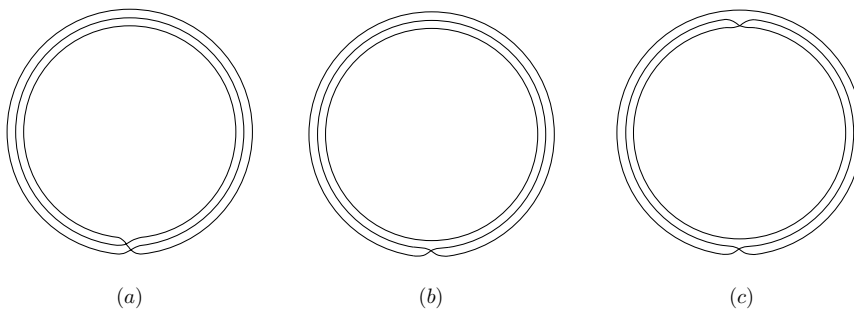


Figure 7. 3-sheeted branched-coverings of a sphere. For the case 3-sheeted branched covering with two branch points, we can repeat our construction, using identification rules as shown in Figure (a). The Figure shows the sectional view from the north pole. Figure (b) shows another gluing rule in which mixed branched and unbranched coverings occur. In Figure (c) in another construction we separated out the two branch points with ramification indices 3 in Figure (a) into four branch points with ramification indices 2.

One can generalize this construction, and create N -sheeted branched (and unbranched) coverings with I branch points by associating permutation elements π_i , $i = 1, \dots, I$ in symmetric group \mathcal{S}_N to each branch points z_i on the sphere. The choice of the permutations π_i 's is basically arbitrary except one constraint to be satisfied by π_i 's:

$$\pi_1 \pi_2 \cdots \pi_I = 1. \quad (16)$$

The reason for this is the following (e.g., Hurwitz 1891). We draw small circles c_i around every branch points z_i , and go around them once starting from an arbitrary non-branch point P on the sphere (Figure 8(a)). This gives the left-hand side of the constraint equation (16). Since we are on the sphere, we can deform this loop (without crossing any branch points) into another loop with the opposite orientation that surrounds small region near the starting point P (Figure 8(b)). Since the point

P is a regular point, this gives the right-hand side of the equation (16). One obtains different coverings according to the various different combinations of π_i 's.

The number of independent coverings created in this way can be counted as

$$\sum'_{\pi_i \in \mathcal{S}_N} \delta(\pi_1 \pi_2 \cdots \pi_I)$$

where \sum' stands for the sum avoiding double counting, and $\delta(p)$ is Kronecker's delta

$$\delta(p) = \begin{cases} 1 & \text{if } p = 1 \\ 0 & \text{otherwise.} \end{cases}$$

We will specify the counting rule \sum' in our specific problem later.

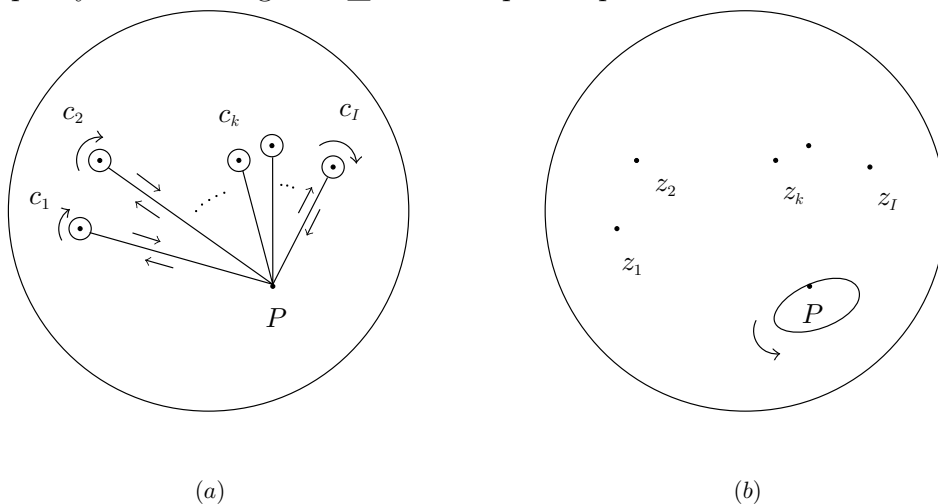


Figure 8. Geometric meaning of the constraint equation (16). We draw small circles c_i around every branch points z_i , and go around them once starting from an arbitrary non-branch point P on the sphere (Figure (a)). This gives the left-hand side of the constraint equation (16). Since we are on the sphere, we can deform this loop (without crossing any branch points) into another loop with the opposite orientation that surrounds small region near the starting point P (Figure (b)). Since the point P is a regular point, this gives the right-hand side of the equation (16).

Now we would like to consider a similar construction for coverings of a plaquette that is needed in this paper. In this case we have to take into account the coverings of the boundary. We assume that our covering sheet(s) have $m (\leq N)$ non-intersecting, mutually independent boundaries B_k ($k = 1, \dots, m$), each homeomorphic to a circle S^1 , and that the boundary of the original plaquette is covered by these boundaries B_k , each L_k times, for some non-negative integer L_k , ($L_1 + L_2 + \cdots + L_m = N$). [Namely, B_k is the L_k -fold cover of the boundary of the original plaquette.]

In the similar way as we specified branch points we can specify this boundary covering in terms of an element $\sigma \in \mathcal{S}_N$ that consists of m cycles of lengths L_1, L_2, \dots, L_m , i.e., $\sigma = (\ell_1 \ell_2 \dots \ell_{L_1})(m_1 m_2 \dots m_{L_2})(\dots)(q_1 q_2 \dots q_{L_m})$. If one goes around the boundary of the original plaquette once in anti-clock-wise direction, one moves on the boundary circles in covering space in a way as specified by σ .

With these preparations we can now construct a branched covering of a plaquette in exactly the same way as in the sphere case. However, here the constraint (16) is replaced by the following one:

$$\pi_1 \pi_2 \dots \pi_I = \sigma^{-1}. \quad (17)$$

The reason is obvious by construction; we just repeat the discussion following equation (16) with the sphere replaced by a plaquette.

We get various mixed branched (and unbranched) coverings under different combinations of π_i 's and σ in the symmetric group \mathcal{S}_N .

In order for this construction to be applicable to our specific problem of orientation modules, we must restrict possible forms of π_i 's and σ . Recall that every orientation modules are labeled by the locally constant function $w_{\mathcal{O}} = \exp(i\pi k_i/N)$, $k_i = 1, \dots, N$, and they constitute an N -sheeted covering of an area of retinal surface. Since, as discussed in the previous section, the neighbouring modules have similar orientation specifications k_i , first we must have the boundary σ as in

$$\sigma = (12 \dots L_1)^{\epsilon_1} (L_1 + 1, \dots, L_1 + L_2)^{\epsilon_2} (\dots) (N - L_m + 1, \dots, N)^{\epsilon_m}, \quad (18)$$

where $\epsilon_i = \pm 1$ ($i = 1, 2, \dots, m$). Secondly, in order to prevent double counting we restrict all π_i to be transpositions $(k\ell) \in \mathcal{S}_N$. This is because as we saw in Figure 7 non-transpositional gluing rule can always be considered as a special case of transpositional gluings where some of the branch points of the ramification indices 2 accidentally come close by. Furthermore in this case we must restrict them to the generators of the symmetric group $(k\ k+1)$, $k = 1, 2, \dots, N-1$, and $(N\ 1)$. The reason for this is locally the neighbouring modules have similar orientation specifications $k_{i\pm 1} = k_i \pm 1$.

Putting all these together, we end up with the expression for the partition function of our orientation modules of module number N per hypercolumn:

$$\mathcal{Z}_N \sim \sum_{I=0}^{\infty} \sum'_{\sigma, \pi_i \in \mathcal{S}_N} \delta(\pi_1 \dots \pi_I \sigma) \int \prod_{i=1}^I d^2 z_i \cdot |\Delta[\mathbf{v}]| e^{-\Delta \mathcal{E}[\mathbf{v}]}. \quad (19)$$

Here the summation $\sum'_{\sigma, \pi_i \in \mathcal{S}_N}$ implies that we restrict π_i to generators $(k \ k+1)$, $k = 1, 2, \dots, N-1$, and $(N \ 1)$ only, and σ as in equation (18) while avoiding any double counting. The energy $\Delta\mathcal{E}[\mathbf{v}]$ is a function of singular points z_i and the boundary condition specified by σ .[‡]

4.2 Most probable modules

Although we are interested in the case where the total module number N (per hyper-column) is large, let us first consider, as an example, the case $N = 5$. First of all, since the cortical surface F has only simple topology, as a covering space its Euler characteristic $\chi(F)$ has to be a positive integer no larger than N ; $\chi(F) = 1, 2, 3, \dots, N$. The case $\chi(F) = N$ corresponds to N unbranched (disconnected) coverings, and $\chi(F) < N$ if the covering is of mixed branched and unbranched one. From the Riemann-Hurwitz formula (15) this restricts the number of (transpositional) singularities $I = 0, 1, 2, \dots, N-1$. In the case $N = 5$ this implies $I = 0, 1, \dots, 4$, and we can easily evaluate possible number of mappings $\sum' \delta(\pi_1 \dots \pi_I \sigma)$ (Table 1). For the boundary condition $\sigma = 1$ we get $\sum' \delta(\pi_1 \pi_2) = 5$, $\sum' \delta(\pi_1 \pi_2 \pi_3 \pi_4) = 15$, and etc. Intuitively these surfaces correspond to coverings connected with double arcs (see Figure 9(b)). In Figure 9(a) we start with $(N =) 5$ unbranched covering-sheets

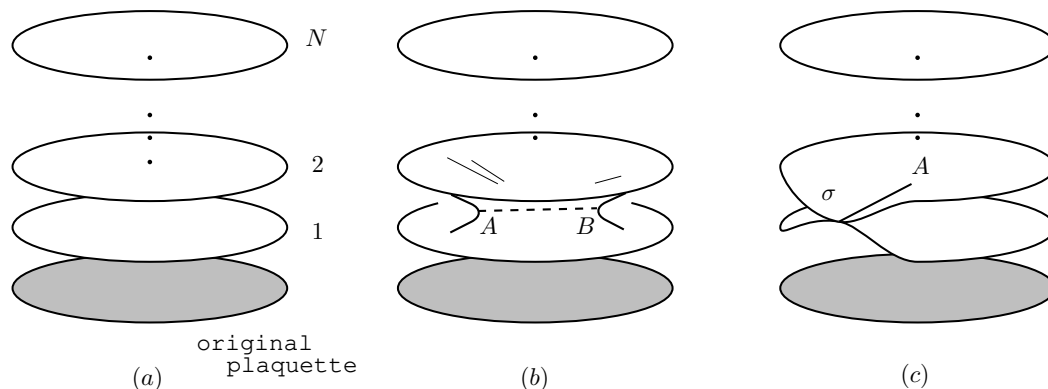


Figure 9. Coverings of a plaquette. In Figure (a) we start with N unbranched covering-sheets of the original plaquette. In Figure (b), we connected the covering-sheets “1” and “2” along a line connecting two singularities A, B , via $\pi_A = \pi_B = (12)$, using a similar rule as explained in Figure 6 in the sphere case. The line connecting the two sheets is called a “double arc”. For the case with the non-trivial boundary condition $\sigma = \sigma(j) \equiv (j, j+1)$ the intuitive picture of the

[‡]The quantity $\Delta[\mathbf{v}]$ is a Jacobian arising from change of functional integration variable $D\mathbf{v} \rightarrow d^2 z_i$ in collective coordinate method.

covering is just like the double arcs stated above except for one singular point that is anchored to $\sigma = (j, j + 1)$ on the boundary (Figure (c)). The latter comprises a branch cut along the line connecting them.

of the original plaquette. In Figure 9(b), we connected the sheets “1” and “2” along a line connecting two singularities A, B , via $\pi_A = \pi_B = (12)$, using a similar rule as explained in Figure 6 in the sphere case. The line connecting the two surface is called a “double arc”. Every term of the type $(i, i + 1) \cdots (i, i + 1)$ appearing in $\pi_1 \pi_2 \cdots \pi_I$ represents such a double arc connecting a pair of covering-sheets “ i ” and “ $i + 1$ ”.

For the case the boundary condition $\sigma = \sigma(j) \equiv (j, j + 1)$, we get $\sum_j \sum' \delta(\pi_1 \sigma(j)) = 5$, $\sum_j \sum' \delta(\pi_1 \pi_2 \pi_3 \sigma(j)) = 15$, and etc. In this case the intuitive picture is just like the double arcs stated above except for one singular point that is anchored to $\sigma = (j, j + 1)$ on the boundary (Figure 9(c)). The latter comprises a branch cut along the line connecting them. The pairs of transpositions that do not contract with σ compose the double arcs as before.

In general we can locate σ anywhere at the boundary. As in the case of singularities π_j we consider the component-decomposition of σ in terms of transpositional elements $(j, j + 1)$. We assume that these components of σ are distributed separately over the boundary in the same order appearing in the transpositional component decomposition in minimal length. The summation $\sum'_{\sigma \in \mathcal{S}_N}$ thus gives rise to factors of $\zeta (= \text{length of the boundary in the unit of } \sigma_0 (= \text{hypercolumn size}))$ in association with each transpositional component $(j, j + 1)$.

Table 1. Combinatorial factors for composing ($N =$)5-fold covering of a small segment of the retinal surface corresponding to one hypercolumn area on the visual cortex. $g = \zeta \mathcal{A}_0 e^{-\Delta \varepsilon_0 / \lambda}$

I	0	1	2	3	4
$\sum' \delta(\pi_1 \cdots \pi_I)$	1		$5\mathcal{A}^2$		$15\mathcal{A}^4$
$\sum_i \sum' \delta(\pi_1 \cdots \pi_I (i, i + 1))$		$5g$		$15g\mathcal{A}^2$	
$\sum_i \sum' \delta(\pi_1 \cdots \pi_I (i, i + 1, i + 2))$			$10g^2$		$20g^2\mathcal{A}^2$
$\sum_i \sum' \delta(\pi_1 \cdots \pi_I (i, i + 1, i + 2, i + 3))$				$10g^3$	
$\sum_{\text{cycles}} \sum' \delta(\pi_1 \cdots \pi_I (12345))$					$10g^4$
$\sum_{\text{pairs}} \sum' \delta(\pi_1 \cdots \pi_I (12)(34))$			$5g^2$		$10g^2\mathcal{A}^2$
$\sum_{\text{pairs}} \sum' \delta(\pi_1 \cdots \pi_I (123)(45))$				$10g^3$	

In the path integral (19) the integration $\int \prod_{i=1}^I d^2 z_i$ also gives rise to factors of \mathcal{A}_0 (= area of the covered plaquette in the unit of σ_0^2) in association with the positional degrees of freedom of the (transpositional) singularities. [For the complete handling of these factors (proportional to the boundary length and area), one actually has to solve stationary point equation associated to (4), and to integrate over all the positions of the singularities and the boundary conditions; the integrand $e^{-\Delta\mathcal{E}}$ depends on those (so-called moduli) parameters in general. The actual integration over the moduli generally gives slightly different contributions rather than the simple multiplications of factors of the area and the boundary length of the plaquette as above. However, here in order to get rough estimation of the path integral we ignore those parameter dependence of the integrand $e^{-\Delta\mathcal{E}}$ ($\Delta\mathcal{E} \equiv \Delta\mathcal{E}_0/\lambda$, cf. equation (10)), and we simply multiply the factors of \mathcal{A}_0 and ζ to its representative value $e^{-\Delta\mathcal{E}_0/\lambda}$ per (transpositional) singularity $(i, i + 1)$.] We combine two factors \mathcal{A}_0 and $e^{-\Delta\mathcal{E}_0/\lambda}$, and write $\mathcal{A} = \mathcal{A}_0 e^{-\Delta\mathcal{E}_0/\lambda}$. In Table 1 instead of the variables ζ, \mathcal{A} we have used g ($\equiv \zeta\mathcal{A}$), \mathcal{A} . In the latter parametrization the power of g equals (minimal) transpositional component number of the boundary condition σ , and that of \mathcal{A} represents twice the number of double arcs in the resulting coverings.

From the Table 1 and the definition of $\mathcal{A} = \mathcal{A}_0 e^{-\Delta\mathcal{E}_0/\lambda}$ one can immediately conclude that appropriate choice of the lateral correlation strength λ in our model suppresses (i.e., $\mathcal{A} < 1$) double-arc contributions. We assume such choice of λ in the following, since that is close to real situation. Then among the resulting \mathcal{A} -independent terms the maximum contribution is obtained from the term with the boundary condition $\sigma = (12345)$ -type if $g > 1$, and from other σ 's if $g < 1$. Since \mathcal{A}_0 is of order 1 and $\zeta \sim 24\sqrt{3}$,[†] (unless the measure λ for the lateral correlation strength is too small) the former boundary condition $\sigma = (12345)$ -type is realized. Hence one gets one orientation-wheel with all orientation directions organized to it. (We assume in the global scale that every transpositional components (separated as a convention for the counting multiplicities) are organized in such a way that each boundary condition σ (with m cycles) corresponds to global m orientation-wheel(s).)

The next largest contribution is from those terms with $\sigma = (1234)$ -type or $\sigma = (123)(45)$ -type, namely, singularities compose either one wheel with fewer orientation-modules or two orientation wheels with three- and two-orientation specifications as in (123) and (45). (When g becomes smaller than 1, the boundary conditions other

[†]The ocular-dominance width $\sim 4\sqrt{3}\sigma_0$ from our previous work (I) has been used.

than $\sigma = (12345)$ -type give dominant contributions. For the detailed classification of this case we would need more precise evaluation of each term in Table 1.)

Table 2. Approximate combinatorial factors for the case that the covering multiplicity N of a retinal surface is large. ($L \equiv \ell_1 + \ell_2 + \dots + \ell_m - m$)

I	0	1	2	3	\dots	L	\dots	N
$\sigma = 1$	1							
$\sigma = (i, i + 1)$		Ng						
$\sigma = (i, i + 1, i + 2)$			$2Ng^2$					
$\sigma = (i, i + 1, i + 2, i + 3)$				$2Ng^3$				
\vdots						\dots		
$\sigma = (123 \dots N)$								$2Ng^{N-1}$
$\sigma = (12)(34)$			$N^2g^2/2$					
$\sigma = (12)(34)(56)$				$N^3g^3/3!$				
\vdots					\dots			
$\sigma = \{\ell_1, \ell_2, \dots, \ell_m; n\}$						Q_σ		

Now we turn to the case N large (Table 2)[‡]. Basic structure of the combinatorial factors remains same as in $N = 5$ case. Since we are not interested in the coverings with multiple double-arcs, we omit the terms with explicit \mathcal{A} dependence in Table 2. For this purpose we have assumed the appropriate choice of the strength measure λ of the lateral correlation $\Lambda_{\vec{r}, \vec{r}^*}$ (so that $\mathcal{A} \equiv \mathcal{A}_0 e^{-\Delta \mathcal{E}_0 / \lambda} < 1$). We also write the boundary condition σ as $\{\ell_1, \ell_2, \dots, \ell_m; n\}$ that consists of cycles of lengths $\ell_1, \ell_2, \dots, \ell_m$ among which n cycles are non-transpositional. Approximate combinatorial factor Q_σ for the general $\sigma = \{\ell_1, \ell_2, \dots, \ell_m; n\}$ is given as

$$Q_\sigma \approx 2^n C_\sigma N g^L \prod_{k=1}^{m-1} \left(1 + \frac{N - L - m + 1}{k} \right), \quad (20)$$

where C_σ is a symmetry factor, e.g., $C_\sigma = 1/m$ if all the cycle-length ℓ_i are equal, $C_\sigma = 1/3$ if $\sigma = \{\ell_1, \ell_2, \ell_1, \ell_2, \ell_1, \ell_2; n\}$, etc., and $C_\sigma = 1$ if there is no symmetry in the configurations of ℓ_i 's, and $L \equiv \sum_{i=1}^m (\ell_i - 1)$.

A larger combinatorial factor is obtained if n is large ($= m$) and σ is non-symmetric (so that $C_\sigma = 1$). Restricting σ to such cases, we evaluate the factor

[‡]In the table we write only representative boundary conditions σ in each row; the summation with respect to i or possible σ 's that fall into the same class as the representative σ is assumed.

Q_σ in the decreasing order of the power g^L . In general there are several configurations σ that have the same power g^L . For instance, in the case $L = N - 4$ we have $\sigma = \{\ell_1, \ell_2, \ell_3, N - \sum_{i=1}^3 \ell_i; 4\}$, $\{\ell_1, \ell_2, N - 1 - \sum_{i=1}^2 \ell_i; 3\}$, $\{\ell_1, N - 2 - \ell_1; 2\}$, and $\{N - 3; 1\}$ (, assuming $\ell_1 \neq \ell_2 \neq \ell_3 > 2$, etc.). The first σ represents four orientation-wheels with all orientation modules belong to one of the four wheels, whereas the remaining σ 's represent three, two, or one orientation-wheel(s) with one, two, or three orientation modules disintegrated from the organized wheel(s). The corresponding combinatorial factors are given as $Q_\sigma = 64Ng^{N-4}$, $48Ng^{N-4}$, $16Ng^{N-4}$, and $2Ng^{N-4}$, respectively. Thus the maximal factor Q_σ is attained in the first σ . In Table 3 we list only those maximal configurations σ together with their combinatorial factors Q_σ for each g^L .

Table 3. Maximal combinatorial factor Q_σ is evaluated for each covering multiplicity N of a small segment of retinal surface. The table shows the values of the factor for various possible coverings specified by “ σ ”.

σ	Q_σ
$\{N; 1\}$	$2Ng^{N-1}$
$\{\ell_1, N - \ell_1; 2\}$	$8Ng^{N-2}$
$\{\ell_1, \ell_2, N - \sum_{i=1}^2 \ell_i; 3\}$	$24Ng^{N-3}$
$\{\ell_1, \ell_2, \ell_3, N - \sum_{i=1}^3 \ell_i; 4\}$	$64Ng^{N-4}$
$\{\ell_1, \ell_2, \ell_3, N - 1 - \sum_{i=1}^3 \ell_i; 4\}$	$160Ng^{N-5}$
$\{\ell_1, \ell_2, \dots, \ell_4, N - \sum_{i=1}^4 \ell_i; 5\}$	$480Ng^{N-6}$
$\{\ell_1, \ell_2, \dots, \ell_5, N - 1 - \sum_{i=1}^5 \ell_i; 6\}$	$1344Ng^{N-7}$
$\{\ell_1, \ell_2, \dots, \ell_5, N - 2 - \sum_{i=1}^5 \ell_i; 6\}$	$3584Ng^{N-8}$
$\{\ell_1, \ell_2, \dots, \ell_6, N - 1 - \sum_{i=1}^6 \ell_i; 7\}$	$10752Ng^{N-9}$
$\{\ell_1, \ell_2, \dots, \ell_6, N - 2 - \sum_{i=1}^6 \ell_i; 7\}$	$30720Ng^{N-10}$
$\{\ell_1, \ell_2, \dots, \ell_7, N - 2 - \sum_{i=1}^7 \ell_i; 8\}$	$84480Ng^{N-11}$
$\{\ell_1, \ell_2, \dots, \ell_7, N - 3 - \sum_{i=1}^7 \ell_i; 8\}$	
$\{\ell_1, \ell_2, \dots, \ell_8, N - 2 - \sum_{i=1}^8 \ell_i; 9\}$	
\vdots	\vdots

From Table 3 one can immediately see that the first $\sigma = \{N; 1\}$ gets maximal Q_σ if $g > 4$. The second boundary condition $\sigma = \{\ell, N - \ell; 2\}$ becomes maximal if $4 > g > 3$. In other words, “all orientations organized into one wheel” becomes

dominant for $g > 4$, and “ ℓ and $N - \ell$ orientation-modules organized respectively into independent wheels” is dominant if $4 > g > 3$. One can generally prove this fact including all lower power g^L -terms as in the followings.

Let $\sigma^* = \{\ell_1, \ell_2, \dots, N - (N - L - m) - \sum_{i=1}^{m-1} \ell_i; m\}$ be a maximal configuration of g^L -terms (with $N - L - m \geq 0$ being the number of disintegrated modules from the wheels). Then using equation (20) and $Q_{\sigma^*} \geq Q_{\sigma}$ for given N, L , one gets

$$3m - 2 \geq 2(N - L) \geq 3m - 5, \quad N - L \geq m. \quad (21)$$

This implies that under the change $L \rightarrow L - 1$ the m -value m_L associated to the maximal configuration is restricted as

$$m_L - \frac{1}{3} \leq m_{L-1} \leq m_L + \frac{5}{3}. \quad (22)$$

Thus we have either $m_{L-1} = m_L$ or $m_L + 1$. In Table 3 both cases are realized. At $L = N - 5, N - 8, N - 11, \dots$ there arise two maximal configurations $\sigma_1^* = \{\ell_1, \ell_2, \dots, N - (N - L - m) - \sum_{i=1}^{m-1} \ell_i; m\}$ and $\sigma_2^* = \{\ell_1, \ell_2, \dots, N - (N - L - m + 1) - \sum_{i=1}^{m-2} \ell_i; m - 1\}$ that have the same maximal factor $Q_{\sigma_1^*} = Q_{\sigma_2^*}$. This situation always occurs for such (N, L, m) that satisfies $2(N - L) = 3m - 5$. (From the restriction $N - L \geq m$, equation (21), the case $L = N - 2$ is excluded from this argument.) Choosing the appropriate configuration $\sigma^* (= \sigma_1^* \text{ or } \sigma_2^*)$ as the maximal configuration for g^L -term if necessary, one can always consider m_L as satisfying $m_{L-1} = m_L + 1$. (See Table 3.)

Now we consider the condition $Q_{\sigma^*}|_L > Q_{\sigma^*}|_{L-1}$ under $m_{L-1} = m_L + 1$ between neighboring maximal σ^* at g^L - and g^{L-1} -terms. From the expression (20) this condition is recast into

$$g > \frac{2(N - L + 1)}{m_L}, \quad (23)$$

for $L \leq N - 2$. However, the right-hand side of this condition is restricted by the inequality (21) as in

$$3 \geq \frac{2(N - L + 1)}{m_L} \geq 3 - \frac{3}{m_L}. \quad (24)$$

Therefore, one concludes that as long as $g > 3$ the relation $Q_{\sigma^*}|_L > Q_{\sigma^*}|_{L-1}$ is always satisfied for all $L (\leq N - 2)$, and the configurations $\sigma = \{\ell, N - \ell; 2\}$ or $\sigma = \{N; 1\}$ get largest combinatorial factors Q_{σ} in all possible σ 's. Obviously, $\sigma = \{N; 1\}$ is dominant if $g > 4$, and so is $\sigma = \{\ell, N - \ell; 2\}$ if $4 > g (> 3)$. This completes the proof.

To summarize we have estimated the partition function (19) of our model that consists of the sum of frequencies (or probabilities) Q_{σ} for the occurrence of various (possible) organizations σ of the orientation-modules. In the sum the organizations

containing M double-arcs (Figure 9(b)) has been shown to have extra $\mathcal{A} = \mathcal{A}_0 e^{-\Delta\mathcal{E}_0/\lambda}$ factor $Q_\sigma \propto g^L \mathcal{A}^M$, where \mathcal{A}_0 , $\Delta\mathcal{E}_0$, λ are the measures for hypercolumn area in the unit of σ_0^2 , average energy per orientation module, and a coefficient in the lateral correlation $\Lambda_{\vec{r}, \vec{r}^*}$, respectively. We have suppressed those (higher order) terms by appropriate choice of λ so that the factor $\mathcal{A} < 1$. Among the remaining non-double-arc organizations (Figure 9(c)), we have proved the following remarkable fact: once g ($\equiv \zeta \mathcal{A}$) exceeds 3, most probable organizations are “all orientation-modules organized into one orientation-wheel (if $g > 4$) or two wheels (if $g < 4$)”. This is remarkable since we do not need any fine-tuning of our parameter λ into special, definite value to obtain this result. Since ζ (= measure of the boundary length of the hypercolumn in the unit of σ_0) is roughly equal to $24\sqrt{3}$ (Yamagishi, 1994), the condition $g > 3$ holds under quite natural circumstance. In contrast, more than 4 orientation-wheels per hypercolumn are not easily realized without fine-tuning of g (or λ -value). Also remarkable is the fact that this result is independent of the total module number N as long as N is large.

5 Summary

In this paper we have considered the modular organization where the feature space consists of infinite (continuous) degrees of freedom. Specifically we have considered the local organization of orientation modules while restricting ourself to a hypercolumn area. Since we do not know the minimal increment (or resolution) of the orientation preference between neighboring modules at low-level visual processing (V1), we proposed here statistical definition for orientation-module boundaries. Each module size in this definition was considered indefinite and was defined only statistically. Their size was considered to be selected in the course of higher-level visual processing. In the organization of such modules semi-local continuity of the orientation preference angles was required for the scheme to work well. In our model of generalized Kohonen’s feature mappings we have successfully realized this scheme. We have also shown in this model that the existence of orientation-wheels observed in visual cortex is a consequence of the celebrated Riemann-Hurwitz formula from (geometric) topology.

This formula from topology came into the game since in our model the holomorphicity plays important role to determine the stationary points of the net, and in two dimensions a holomorphic mapping is (locally) conformal. Hence the topological

property has turned out to play essential role.

Within the scope of the same topological argument we have discussed the most adequate number for orientation-wheels per hypercolumn. We have estimated it by evaluating the partition function \mathcal{Z}_N , equation (19). The resulting most probable orientation-wheel consists of all orientation modules organized monotonically with respect to orientation angles if the lateral correlation strength λ is chosen in such a way that $g(= \zeta \mathcal{A}_0 e^{-\Delta \mathcal{E}_0 / \lambda}$, where ζ [$\approx 24\sqrt{3}$ from the previous work I] being a measure of the boundary-length of the hypercolumn region) exceeds 4 and $\mathcal{A}_0 e^{-\Delta \mathcal{E}_0 / \lambda} < 1$. Even if that is not the case, if g exceeds 3, we have two wheels consisting of all orientations. In contrast, more than four orientation-wheels per hypercolumn are hard to realize without fine-tuning of the parameter g . This is remarkable since we have the adequate organization of the orientation-wheels independently of the minimal increment ($\approx \frac{180^\circ}{N}$) of the orientation angles. This number of orientation-wheels is also consistent with the observed result on macaque monkeys. This property remains true under the change of N as long as N large without re-tuning the parameter λ (hence g -value)[†].

We have a couple of important issues left untouched in this paper. Basically what we have considered here are the things that could be handled with tools only from topology. However, for the analysis of the real cortical surface, such as global organization of the orientation modules over the broad range, we have to go beyond the topology. This is very difficult but important issue. Another thing to be clarified is the selection mechanism of the iso-orientation width (or increment) in the organized wheels that we assumed as higher-cortical function. We would like to return to these issues in the future publications.

Part of this work was performed under the auspices of the U.S. Department of Energy by the Lawrence Livermore National Laboratory under Contract W-7405-ENG-48 with the University of California.

[†]The most of the result of this paper is correct if N is larger than 10, approximately.

References

- Bonhoeffer, T., & Grinvald, A. (1993). The layout of iso-orientation domains in area 18 of cat visual cortex: optical imaging reveals a pinwheel-like organization. *Journal of Neuroscience*, **13**, 4157-4180.
- Blasdel, G.G. (1992). Orientation selectivity, preference, and continuity in monkey striate cortex. *Journal of Neuroscience*, **12**, 3139-3161.
- Daugman, J.G. (1985). Uncertainty relation for resolution in space, spacial frequency, and orientation optimized by two-dimensional visual cortical filters. *Journal of the Optical Society of America*, **A2**, 1160-1169.
- Fitzpatrick, D., Lund, J.S., & Blasdel, G.G. (1985). Intrinsic connections of macaque striate cortex: afferent and efferent connections of lamina 4C. *Journal of Neuroscience*, **5**, 3329-3349.
- Gilbert, C.D., & Wiesel, T.N. (1983). Clustered intrinsic connections in cat visual cortex. *Journal of Neuroscience*, **3**, 1116-1133.
- Gilbert, C.D., & Wiesel, T.N. (1989). Columnar specificity of intrinsic horizontal and corticocortical connections in cat visual cortex. *Journal of Neuroscience*, **9**, 2432-2442.
- Griffiths, P., & Harris, J. (1978). Principles of algebraic geometry. New York, NY: John Wiley & Sons.
- Hawken, M.J., & Parker, A.J. (1987). Spacial properties of neurons in the monkey striate cortex. *Proceedings of the Royal Society of London*, **B231**, 251-288.
- Hubel, D.H., & Wiesel, T.N. (1977). Functional architecture of macaque monkey visual cortex. *Proceedings of the Royal Society of London*, **B198**, 1-59.
- Hurwitz, A. 1891. Ueber Riemann'sche Flächen mit gegebenen Verzweigungspunkten. *Mathematische Annalen*, **39**, 1-60.
- Jones, J.P., & Palmer, L.A. (1987). An evaluation of the two-dimensional Gabor-filter model of simple receptive fields in cat striate cortex. *Journal of Neurophysiology*, **58**, 1233-1258.
- Kohonen, T. (1982). Self-organized formation of topologically correct feature maps. *Biological Cybernetics*, **43**, 59-69.

- Kohonen, T. (1989). Self-organization and associative memory (3rd ed.). New York, NY: Springer-Verlag.
- Matsubara, B.A., Cynader, M.S., & Swindale, N.V. (1987). Anatomical properties and physiological correlates of intrinsic connections in cat area 18. *Journal of Neuroscience*, **7**, 1428-1446.
- McGuire, B.A., Gilbert, C.D., Rivlin, P.K., & Wiesel, T.N. (1991). Targets of horizontal connections in macaque primary visual cortex. *Journal of Comparative Neurology*, **305**, 370-392.
- Obermayer, K., & Blasdel, G.G. (1993). Geometry of orientation and ocular dominance columns in monkey striate cortex. *Journal of Neuroscience*, **13**, 4114-4129.
- Obermayer, K., Ritter, H., & Schulten, K. (1990). A principle for the formation of the spatial structure of cortical feature maps. *Proceedings of the National Academy of Science USA*, **87**, 8345-8349.
- Obermayer, K., Blasdel, G.G., & Schulten, K. (1992). Statistical-mechanical analysis of self-organization and pattern formation during the development of visual maps, *Physical Review*, **A45**. 7568-7589.
- Ritter, H., & Schulten, K. (1986). On the stationary state of Kohonen's self-organizing mapping. *Biological Cybernetics*, **54**, 99-106.
- Yamagishi, K. (1994). Spontaneous symmetry breaking and the formation of columnar structures in the primary visual cortex. *Network*, **5**, 61-73.

Figure Legends

Figure 1. Ice-cube model of orientation columns by Hubel and Wiesel. Orientation columns are regularly embedded in R, L ocular dominance area.

Figure 2. Examples of a folding map (*a*) and a line degeneracy (*b*). Slightly separated appearance of the leaves in the folding map (*a*) is for the sake of visibility. These mappings can occur when the Jacobian $J(\vec{v}) = \det(\partial v_i(\vec{r})/\partial r_j)$ of the mapping $\vec{v}(\vec{r})$ between retinal and the corresponding cortical surfaces vanishes.

Figure 3. Multiple winning points on a folding cover. When one encounters a folding cover of the retinal surface, because of the “winner-takes-all” rule each leaf $i - 1$, i , $i + 1$ of the folding cover has to have different orientation preference $w_{\mathcal{O}}(\vec{r}^*)$.

Figure 4. Labeling of a multiple covering (unfolded view). As in the case of folding covers (Figure 3) the “winner-takes-all” rule enforces different labeling $w_{\mathcal{O}} = e^{i\pi k_i/N}$, $k_i \neq k_j$, for each covering-sheet of retinal surface in general multiple coverings.

Figure 5. An unbranched covering of a torus. We write a plaquette for a torus, assuming identification of like-labeled edges in each side (Figure (*a*)). An unbranched N -sheeted covering (Figure (*b*)) is a collection of N such objects glued together along like-labeled edges. Then one identifies each horizontal edges, and wraps up the torus with the resulting cylinder by putting one end of the cylinder in the other end until the circumferences match up with the original torus (Figure (*c*)).

Figure 6. A branched covering of a sphere. We start with a 2-sheeted unbranched covering of S^2 , and name the covering sheets “1” and “2”. To make from this a branched covering, we pick two points (A, B) on the sphere and cut the covering sheets along the straight line connecting these two points (Figure (*a*)). Then we identify one edge of the sheet “1” with the edge of the sheet “2” on the other side of the cut and the remaining edge of the sheet “1” with that of the sheet “2”, i.e., we identify the like-labeled edges p, q in the Figure (*a*). The resulting covering is branched; the two points A, B we picked are branch points (of index 2). To see its topologically equivalent surface, we peel off the outer sphere, and paste it back along the edges p, q as prescribed (Figure (*b*)).

Figure 7. 3-sheeted branched-coverings of a sphere. For the case 3-sheeted branched

covering with two branch points, we can repeat our construction, using identification rules as shown in Figure (a). The Figure shows the sectional view from the north pole. Figure (b) shows another gluing rule in which mixed branched and unbranched coverings occur. In Figure (c) in another construction we separated out the two branch points with ramification indices 3 in Figure (a) into four branch points with ramification indices 2.

Figure 8. Geometric meaning of the constraint equation (16). We draw small circles c_i around every branch points z_i , and go around them once starting from an arbitrary non-branch point P on the sphere (Figure (a)). This gives the left-hand side of the constraint equation (16). Since we are on the sphere, we can deform this loop (without crossing any branch points) into another loop with the opposite orientation that surrounds small region near the starting point P (Figure (b)). Since the point P is a regular point, this gives the right-hand side of the equation (16).

Figure 9. Coverings of a plaquette. In Figure (a) we start with N unbranched covering-sheets of the original plaquette. In Figure (b), we connected the covering-sheets “1” and “2” along a line connecting two singularities A, B , via $\pi_A = \pi_B = (12)$, using a similar rule as explained in Figure 6 in the sphere case. The line connecting the two sheets is called a “double arc”. For the case with the non-trivial boundary condition $\sigma = \sigma(j) \equiv (j, j + 1)$ the intuitive picture of the covering is just like the double arcs stated above except for one singular point that is anchored to $\sigma = (j, j + 1)$ on the boundary (Figure (c)). The latter comprises a branch cut along the line connecting them.

[Figures are embedded in the text.]